Potential energy states and mechanical properties of thermally cycled binary glasses

Nikolai V. Priezjev[1,a]

[1]Department of Mechanical and Materials Engineering, Wright State University, Dayton, Ohio 45435, USA; and National Research University Higher School of Economics, Moscow 101000, Russia
[a]Address all correspondence to this author. e-mail: nikolai.priezjev@wright.edu
Received: 24 January 2019; accepted: 2 April 2019

The influence of repeated thermal cycling on mechanical properties, structural relaxation, and evolution of the potential energy in binary glasses is investigated using molecular dynamics simulations. The authors consider a binary mixture annealed with different cooling rates and then exposed to one thousand thermal cycles at constant pressure. It is found that during the first few hundred transient cycles, the potential energy minima after each cycle gradually decrease and the structural relaxation proceeds through collective, irreversible displacements of atoms. With increasing cycle number, the amplitudes of the volume and potential energy oscillations are significantly reduced, and the potential energy minima saturate to a constant value that depends on the thermal cycling amplitude and the initial cooling rate. In the steady state, the glasses thermally expand and contract but most of the atoms return to their cages after each cycle, similar to limit cycles found in periodically driven amorphous materials. The results of tensile tests demonstrate that the elastic modulus and the yielding peak, evaluated after the thermal treatment, acquire maximum values at a particular thermal cycling amplitude, which coincides with the minimum of the potential energy.

Introduction

The design of novel strategies and optimization of thermal and mechanical treatments of metallic glasses is important for accessing a broad range of states with improved physical and mechanical properties [1]. It is generally accepted that an elementary plastic event in disordered solids involves a collective rearrangement of a small group of atoms or a shear transformation [2, 3]. Owing to lack of crystalline order, the plastic deformation of metallic glasses typically occurs through highly localized shear bands, which leads to catastrophic failure [4]. In recent years, a number of methods were proposed to enhance plasticity of metallic glasses, such as addition of chemical heterogeneities [5, 6] or a soft second phase [7]. A less intrusive way to tune the amorphous structure is to apply cryogenic thermal cycling that can induce rejuvenation due to heterogeneity in the local thermal expansion and therefore improve plasticity [8, 9, 10, 11, 12, 13]. Using atomistic simulations, it was recently shown that internal stresses due to thermal expansion can in principle trigger a plastic event in sufficiently large systems [14].

It was originally demonstrated using molecular dynamics (MD) simulations that the effects of annealing and aging on atomic glasses can be reversed by mechanical rejuvenation, which expels the system from the deep energy minimum [15]. Later, it was found that a single subyield cycle overages the glass by decreasing its potential energy, whereas a shear cycle with large strain rejuvenates the glass and increases its potential energy [16]. More recently, a number of studies have explored the influence of periodic shear deformation on the energy states, particle dynamics, and mechanical properties of amorphous materials [17, 18, 19, 20, 21, 22, 23, 24, 25, 26, 27, 28, 29]. In particular, it was shown by athermal quasistatic simulations that, following a number of training cycles, the glassy systems evolve into periodic limit cycles, where particle trajectories become exactly reversible, despite large-scale collective displacements during each cycle [19, 21]. Most recently, the structural relaxation in binary glasses subjected to periodic temperature variations below the glass transition was investigated using MD simulations [30]. It was found that the potential energy after one hundred cycles acquires a distinct

minimum as a function of the thermal cycling amplitude, which correlates with the largest yield stress at the same amplitude [30]. It remains unclear, however, whether these results depend on the number of thermal cycles and details of the thermal treatment protocol.

In this work, we carried out MD simulations to study the effect of thermal cycling on the evolution of the potential energy and mechanical properties of binary glasses. The amorphous samples were initially prepared by cooling across the glass transition to a low temperature with different rates. It will be shown that after a number of transient cycles, binary glasses attain low energy states and the particle dynamics becomes nearly reversible. We find that the minimum of the potential energy after one thousand cycles and the maximum of the stress overshoot and elastic modulus occur at the same thermal cycling amplitude.

This article is structured as follows. The description of MD simulations including parameter values, annealing procedure, and temperature variation protocol are given in the next section. The numerical results for the potential energy time series, nonaffine displacements, and mechanical properties are presented in section "Results". The conclusions and outlook are provided in the last section.

MD simulations

In this study, we consider a binary (80:20) mixture model to represent a bulk metallic glass. This model was originally introduced by Kob and Andersen (KA) [31] and its parametrization is similar to the model proposed by Weber and Stillinger to describe the amorphous metal alloy $Ni_{80}P_{20}$ [32]. In the KA model, the interaction between any two atoms of types $\alpha, \beta = A, B$ is specified by the truncated Lennard-Jones (LJ) potential,

$$V_{\alpha\beta}(r) = 4\varepsilon_{\alpha\beta}\left[\left(\frac{\sigma_{\alpha\beta}}{r}\right)^{12} - \left(\frac{\sigma_{\alpha\beta}}{r}\right)^{6}\right] \quad , \qquad (1)$$

with the following values of the LJ parameters: $\varepsilon_{AA} = 1.0$, $\varepsilon_{AB} = 1.5$, $\varepsilon_{BB} = 0.5$, $\sigma_{AA} = 1.0$, $\sigma_{AB} = 0.8$, $\sigma_{BB} = 0.88$, and $m_A = m_B$ [31]. The cutoff radius for the LJ potential is set to $r_{c,\alpha\beta} = 2.5\sigma_{\alpha\beta}$ throughout the study. For clarity, we express all physical quantities in terms of the reduced LJ units of length, mass, energy, and time as follows: $\sigma = \sigma_{AA}$, $m = m_A$, $\varepsilon = \varepsilon_{AA}$, and $\tau = \sigma\sqrt{m/\varepsilon}$. The system consists of 48,000 large atoms of type A and 12,000 small atoms of type B, and, hence, the total number of atoms is $N_{tot} = 60,000$. For each configuration of atoms, the total force on each atom from its neighbors was computed using Eq. (1), and the atom positions and velocities were advanced using the velocity Verlet algorithm [33] with the time step $\Delta t_{MD} = 0.005\tau$ [34].

We next briefly describe the annealing process and the temperature variation protocols. First, the system was allowed to equilibrate in a periodic box at zero pressure and temperature of $0.7\varepsilon/k_B$. This temperature is well above the glass transition temperature of the KA model $T_g \approx 0.435\varepsilon/k_B$ at the atomic density $\rho = \rho_A + \rho_B = 1.2\sigma^{-3}$ [31]. The temperature, indicated by T_{LJ}, was maintained by the Nosé–Hoover thermostat with a damping term [33, 34]. Following the equilibration procedure, the binary mixture was annealed into the glass phase with the cooling rates $10^{-2}\ \varepsilon/k_B\tau$, $10^{-3}\ \varepsilon/k_B\tau$, $10^{-4}\ \varepsilon/k_B\tau$, and $10^{-5}\ \varepsilon/k_B\tau$. A representative snapshot of the simulated system is shown in Fig. 1 for the cooling rate of $10^{-2}\ \varepsilon/k_B\tau$. Next, the temperature was varied piecewise linearly with the maximum values $T_{LJ} = 0.1\varepsilon/k_B$, $0.2\varepsilon/k_B$, $0.25\varepsilon/k_B$, $0.3\varepsilon/k_B$, $0.35\varepsilon/k_B$, and $0.4\varepsilon/k_B$ with respect to the reference temperature of $10^{-2}\ \varepsilon/k_B\tau$. The period of thermal cycling was set to $T = 5000\tau$. The postprocessing analysis was performed using accumulated data for the system dimensions, temperature, pressure components, potential energy, and atomic configurations.

Results

We begin the discussion of the results by presenting in Fig. 2 the time dependence of the potential energy for binary glasses annealed across the glass transition to $T_{LJ} = 0.01\varepsilon/k_B$ with cooling rates $10^{-2}\ \varepsilon/k_B\tau$, $10^{-3}\ \varepsilon/k_B\tau$, $10^{-4}\ \varepsilon/k_B\tau$, and $10^{-5}\ \varepsilon/k_B\tau$ and aged at this temperature during the time interval of $5 \times 10^6\ \tau$. As is evident, the potential energy levels become lower when cooling is slower, because the system has more time to explore various minima in the potential energy landscape when
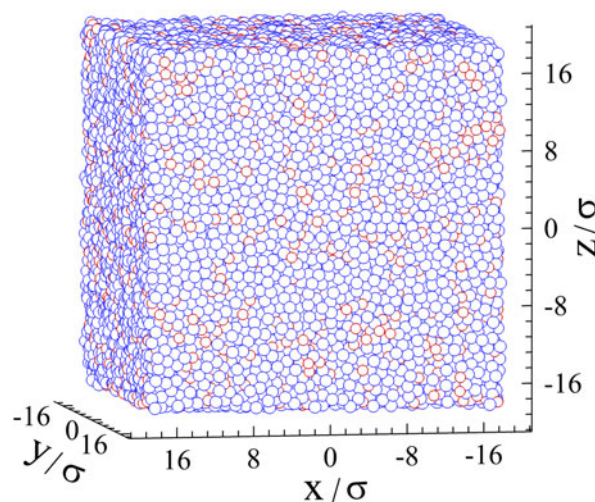

Figure 1: A snapshot of the binary Lennard-Jones glass (60,000 atoms) after annealing from a liquid state to the temperature $T_{LJ} = 0.01\varepsilon/k_B$ with the cooling rate of $10^{-2}\ \varepsilon/k_B\tau$. Atoms of types A and B are indicated by large blue and small red spheres, respectively.
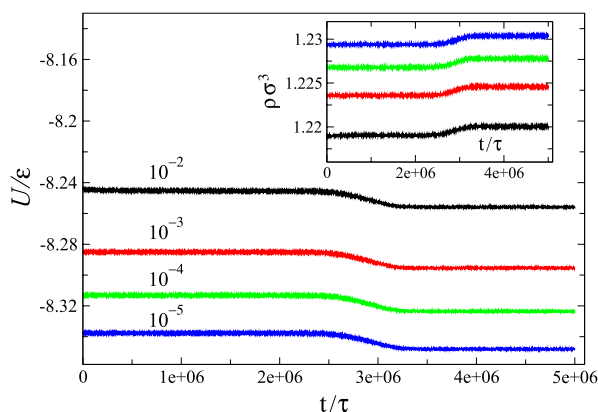
Figure 2: The time dependence of the potential energy per atom, U/ε, at $T_{LJ} = 0.01\varepsilon/k_B$ and $P = 0$ during the time interval of $5 \times 10^6 \, \tau$. The glasses were initially prepared with the cooling rates of $10^{-2} \, \varepsilon/k_B\tau$ (black), $10^{-3} \, \varepsilon/k_B\tau$ (red), $10^{-4} \, \varepsilon/k_B\tau$ (green), and $10^{-5} \, \varepsilon/k_B\tau$ (blue). The time evolution of the average density for the same samples is shown in the inset. The initial cooling rates are $10^{-2} \, \varepsilon/k_B\tau$, $10^{-3} \, \varepsilon/k_B\tau$, $10^{-4} \, \varepsilon/k_B\tau$, and $10^{-5} \, \varepsilon/k_B\tau$ (from bottom to top).

Figure 3: The temperature T_{LJ} (in units of ε/k_B) during the first five periods, $T = 5000\tau$, for the temperature amplitudes $0.1\varepsilon/k_B$ (red), $0.2\varepsilon/k_B$ (green), $0.3\varepsilon/k_B$ (blue), and $0.4\varepsilon/k_B$ (black). The horizontal dashed line indicates the critical temperature of $0.435\varepsilon/k_B$.

approaching the glass transition temperature. This effect was repeatedly observed in MD simulations of glass formers annealed below the glass transition temperature [35]. Somewhat surprisingly, it can be seen in Fig. 2 that in all cases, the potential energy remains nearly constant during $2.5 \times 10^6 \, \tau$ and then gradually crosses over to slightly lower levels during the time interval of about $10^6 \, \tau$. The inset in Fig. 2 shows that the decrease in energy is accompanied with densification of glasses, because simulations are carried out at constant pressure. The analysis of the atomic structure, based on the pair distribution functions, did not reveal any crystallization or enhanced short range order after samples become denser (not shown). We comment that most of the long-time MD simulations of the KA model were performed either at constant volume or near T_g, where the effect presented in Fig. 2 is absent [36]. In the future, it might be instructive to perform a more careful analysis of the structure during aging process at constant pressure and low temperature.

As described in the previous section, the glasses were first annealed at constant pressure to the low temperature of $0.01\varepsilon/k_B$ with cooling rates $10^{-2} \, \varepsilon/k_B\tau$, $10^{-3} \, \varepsilon/k_B\tau$, $10^{-4} \, \varepsilon/k_B\tau$, and $10^{-5} \, \varepsilon/k_B\tau$. The thermal treatment was then applied by repeatedly heating and cooling the samples during 1000 cycles with the period $T = 5000\tau$. Examples of the temperature profiles measured during the first five cycles are presented in Fig. 3. During each cycle, the system gradually expands upon heating to the maximum temperature T_{LJ} and then cooled with the effective rate of about $2T_{LJ}/T$. When the glass temperature become higher, the probability of thermally activated rearrangements of atoms increases, thus leading to structural relaxation over consecutive cycles. In this study, the maximum amplitude of thermal cycling is $T_{LJ} = 0.4\varepsilon/k_B$, just below $T_g \approx$
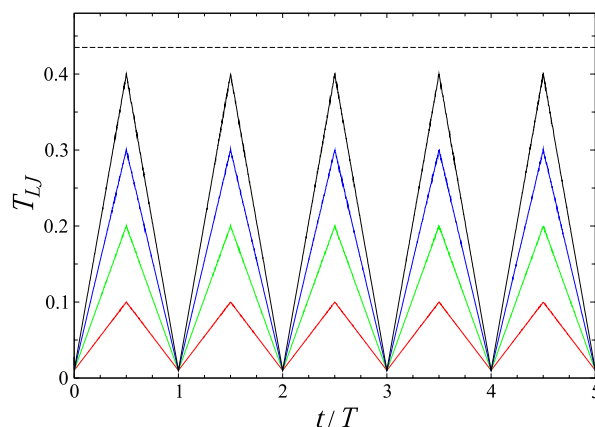
$0.435\varepsilon/k_B$, as it is expected that cycling with higher thermal amplitudes will result in melting and repeated quenching to the solid phase across the glass transition.

The representative potential energy series during 1000 thermal cycles are shown in Fig. 4 for poorly annealed ($10^{-2} \, \varepsilon/k_B\tau$) and in Fig. 5 for well-annealed ($10^{-5} \, \varepsilon/k_B\tau$) glasses and maximum temperatures $0.1\varepsilon/k_B$ and $0.35\varepsilon/k_B$. For reference, the potential energies for aged glasses at constant temperature $T_{LJ} = 0.01\varepsilon/k_B$ are also presented in Figs. 4 and 5 by the red curves, the same data as in Fig. 2 for samples annealed with cooling rates $10^{-2} \, \varepsilon/k_B\tau$ and $10^{-5} \, \varepsilon/k_B\tau$. It can be observed in Fig. 4(a) that the amplitude of the potential energy oscillations is relatively large during the first 300 cycles, and then it is gradually reduced by a factor of about three during the next hundred cycles until a steady state is attained. Note that the potential energy minima after every cycle (the lower envelope of the energy oscillations) gradually decreases during the first 500 cycles but then it remains constant in steady state. We also comment that similar features, as shown in Fig. 4(a), are present for the variation of the total volume, i.e., the system becomes denser and the amplitude of the volume oscillations is reduced in the steady state (Fig. S1).

The thermal cycling with the higher maximum temperature $0.35\varepsilon/k_B$, shown in Fig. 4(b), results in qualitatively similar response; however, the transition to the steady state occurs after about 200 cycles. Note that in both cases presented in Fig. 4, the onset of the potential energy decrease in thermally cycled glasses appears sooner than for the sample aged at the low temperature $0.01\varepsilon/k_B$. The same conclusions can be deduced from the potential energy series for the well-annealed glass (cooling rate $10^{-5} \, \varepsilon/k_B\tau$) shown in Fig. 5, except that the energy levels for the aged glass (red curves) remain closer to the energy minima of thermally cycled glasses. We comment that
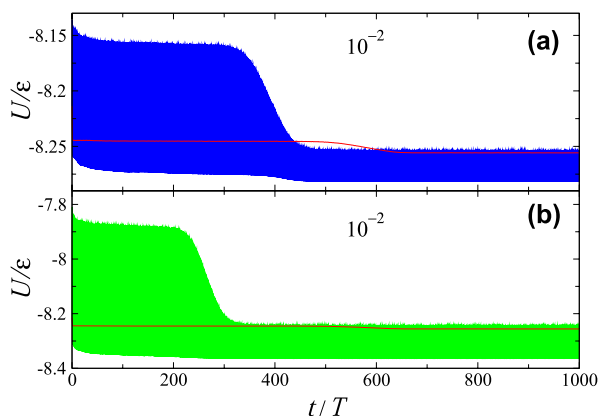
Figure 4: The potential energy during 1000 thermal cycles with maximum temperatures: (a) $0.1\varepsilon/k_B$ (blue) and (b) $0.35\varepsilon/k_B$ (green). The potential energy of the glass aged at $T_{LJ} = 0.01\varepsilon/k_B$ is denoted by red curves (the same data as in Fig. 2). The vertical scales in both panels are different. The oscillation period is $T = 5000\tau$. The glass was initially prepared with the cooling rate of 10^{-2} $\varepsilon/k_B\tau$.
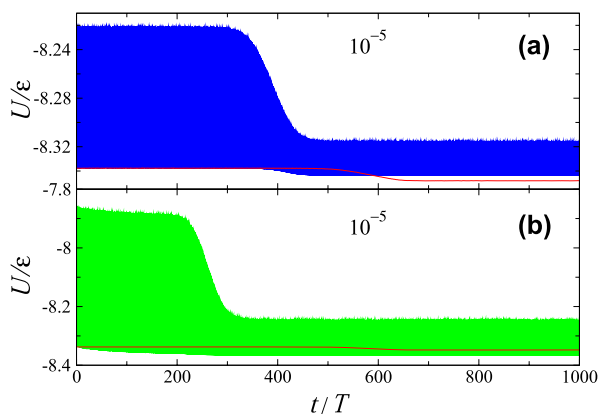

Figure 5: The potential energy series for the thermally cycled glass with maximum temperatures: (a) $0.1\varepsilon/k_B$ (blue) and (b) $0.35\varepsilon/k_B$ (green). Before the thermal treatment, the glass was annealed with the cooling rate of 10^{-5} $\varepsilon/k_B\tau$. Red curves denote the potential energy for the glass aged at $T_{LJ} = 0.01\varepsilon/k_B$ (the same data as in Fig. 2). The period of thermal oscillations is $T = 5000\tau$. The vertical scales are different in both cases.

the characteristic decay of the amplitude of potential energy oscillations after several hundred cycles was observed in all samples and all thermal cycling amplitudes considered in this study; however, they are omitted here for brevity.

The summary of the data for the potential energy minima after each thermal cycle is presented in Fig. 6 for binary glasses cooled with the rates 10^{-2} $\varepsilon/k_B\tau$, 10^{-3} $\varepsilon/k_B\tau$, 10^{-4} $\varepsilon/k_B\tau$, and 10^{-5} $\varepsilon/k_B\tau$. In all panels, the potential energy for glasses aged at constant temperature of $0.01\varepsilon/k_B$ is indicated by the black curves (the same data as in Fig. 2). On inspection of the data in Fig. 6, the common trend emerges for all samples cycled with the maximum temperatures $0.1\varepsilon/k_B \leq T_{LJ} \leq 0.35\varepsilon/k_B$; namely, the potential energy gradually decreases during several hundred cycles until a steady state is reached. Typically, the onset of the
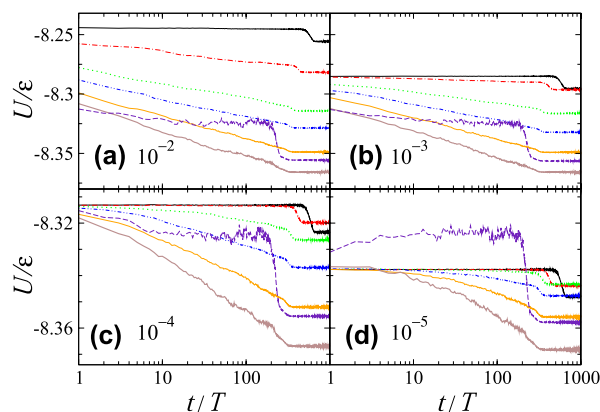

Figure 6: The potential energy minima after each thermal cycle for glasses initially annealed with cooling rates (a) 10^{-2} $\varepsilon/k_B\tau$, (b) 10^{-3} $\varepsilon/k_B\tau$, (c) 10^{-4} $\varepsilon/k_B\tau$, and (d) 10^{-5} $\varepsilon/k_B\tau$. The potential energy for samples at constant temperature of $0.01\varepsilon/k_B$ is indicated by solid black curves (the same data as in Fig. 2). The energy minima for thermally cycled glasses with the maximum temperature of $0.1\varepsilon/k_B$ (dashed-dotted red), $0.2\varepsilon/k_B$ (dotted green), $0.25\varepsilon/k_B$ (dashed-double dotted blue), $0.3\varepsilon/k_B$ (orange), $0.35\varepsilon/k_B$ (dark brown), and $0.4\varepsilon/k_B$ (dashed indigo). Note that the vertical scales in the upper and lower panels are different.

steady state with a well-defined level of the potential energy occurs sooner for higher thermal cycling amplitudes. Except for the cases $T_{LJ} = 0.1\varepsilon/k_B$ and $0.2\varepsilon/k_B$ in Fig. 6(d), the potential energy in the steady state is lower for higher thermal amplitudes.

Overall, the results in Fig. 6 resemble the behavior of the potential energy in glasses during cyclic shear, where it was shown that a certain number of training cycles are required to reach a steady state of periodic deformation [18, 19, 24]. In particular, it was demonstrated that with increasing strain amplitude below yield, the number of transient cycles increases and the potential energy level becomes deeper, leading to steady states where particle trajectories become exactly reversible at zero temperature [18, 19, 24]. However, this analogy does not cover all aspects of thermally cycled glasses, because MD simulations are performed at finite temperature and the number of thermal cycles required to reach a steady state decreases with increasing thermal cycling amplitude, as shown in Fig. 6. We finally note that the potential energy curves for all four samples thermally cycled with the maximum temperature $T_{LJ} = 0.4\varepsilon/k_B$ are nearly the same after about 10 cycles (Fig. 6).

Additional details of the structural relaxation process during thermal treatment can be obtained by examining the so-called nonaffine displacements of atoms. Recall that the nonaffine measure quantifies a displacement of a particular atom with respect to its neighbors during some time interval. This quantity can be evaluated numerically as follows. First, a transformation matrix $\mathbf{J}_i$, which describes a linear transformation of neighbors of the i-th atom during the time

interval Δt, needs to be computed [37]. Then, the nonaffine measure is determined as follows:

$$
\begin{aligned}
D^2(t, \; \Delta t) \\
= \frac{1}{N_i} \sum_{j=1}^{N_i} \left\{ \mathbf{r}_j(t + \Delta t) - \mathbf{r}_i(t + \Delta t) - \mathbf{J}_i \left[\mathbf{r}_j(t) - \mathbf{r}_i(t) \right] \right\}^2 ,
\end{aligned} \quad (2)
$$

where the sum is carried over neighboring atoms that are located closer than 1.5σ to the i-th atom. In the last few years, the numerical analysis of nonaffine displacements was performed for cyclically sheared [22, 23, 25, 27, 28], compressed [38], and thermally cycled [30] glasses. Interestingly, it was found that the yielding transition in poorly annealed [28] and well-annealed [25] glasses occurs after a certain number of cycles and it is associated with the formation of a system spanning shear band that consists of atoms with relatively large nonaffine displacements. On the other hand, a reduction in size of clusters of atoms with large nonaffine displacements upon mechanical annealing signifies an approach to a regime of reversible deformation where most atoms return to their cages after each cycle [22, 23, 25, 27, 28, 38].

The sequence of spatial configurations of atoms with large nonaffine displacements during one cycle is presented in Fig. 7 for poorly annealed (10^{-2} $\varepsilon/k_B\tau$) and in Fig. 8 for well-annealed (10^{-5} $\varepsilon/k_B\tau$) glasses. In both cases, the maximum temperature during each cycle is $0.35\varepsilon/k_B$. It can be observed in Fig. 7 that during the first cycle, most of the atoms in the rapidly quenched glass undergo large nonaffine displacements and leave their cages. The typical cage size is about $r_c \approx 0.1\sigma$. With increasing cycle number, the characteristic size of clusters of mobile atoms is reduced, and only a few isolated atoms are present after the last cycle, indicating a nearly reversible dynamics. It was recently shown that the appearance of several mobile atoms in glasses subjected to multiple subyield shear cycles does not necessarily imply diffusive motion, because these atoms can jump back and forth between neighboring cages [22, 23]. A qualitatively similar behavior is reported in Fig. 8 for the well-annealed glass, except that the typical size of clusters of atoms with large nonaffine displacements after the first cycle is significantly reduced.

Altogether, the analysis of nonaffine displacements suggests that during the first few hundred cycles, the thermal treatment induces collective, irreversible rearrangements of atoms during each cycle that leads to progressively lower potential energies. Once a steady state with a certain energy level is attained, the particle dynamics becomes nearly reversible. In other words, after a certain number of transient cycles, the glass is represented by a particular configuration of atoms that expand on heating but return to their cages after each cycle. This situation is similar to the so-called limit cycles reported in athermal quasistatic simulations of amorphous solids, where
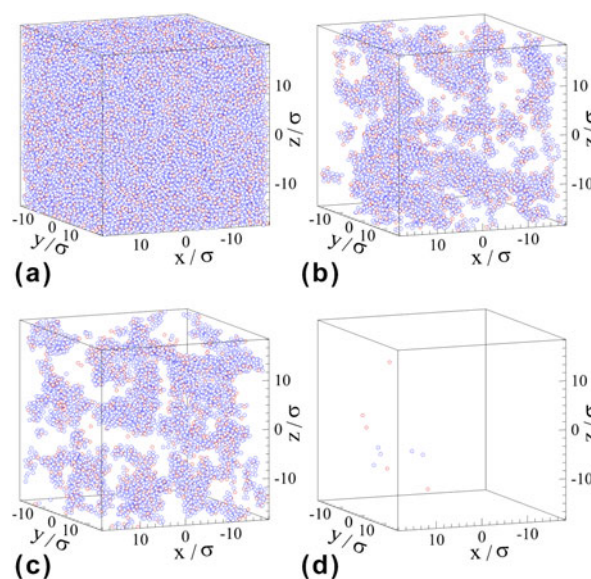

Figure 7: Spatial configurations of atoms with large nonaffine measure (a) $D^2(0, T) > 0.04\sigma^2$, (b) $D^2(99T, T) > 0.04\sigma^2$, (c) $D^2(199T, T) > 0.04\sigma^2$, and (d) $D^2(999T, T) > 0.04\sigma^2$. The sample was initially annealed with the cooling rate of 10^{-2} $\varepsilon/k_B\tau$ and then subjected to thermal cycling with the maximum temperature of $0.35\varepsilon/k_B$.
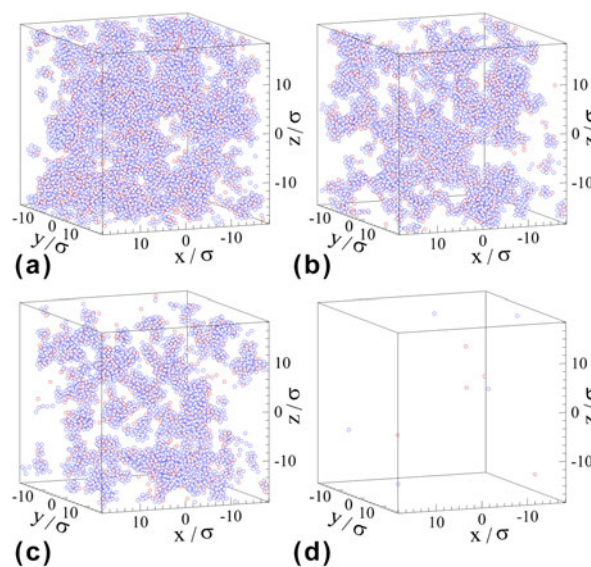

Figure 8: Positions of atoms with large nonaffine displacements (a) $D^2(0, T) > 0.04\sigma^2$, (b) $D^2(99T, T) > 0.04\sigma^2$, (c) $D^2(199T, T) > 0.04\sigma^2$, and (d) $D^2(999T, T) > 0.04\sigma^2$. The maximum temperature of thermal oscillations is $0.35\varepsilon/k_B$. The binary glass was initially prepared with the cooling rate 10^{-5} $\varepsilon/k_B\tau$.

the particle trajectories become exactly reversible after one or more shear cycles [18, 19, 24].

We next examine the effect of thermal cycling on mechanical properties of binary glasses by applying a tensile strain with the rate of $\dot{\varepsilon}_{xx} = 10^{-5}\tau^{-1}$ at $T_{LJ} = 0.01\varepsilon/k_B$ and $P = 0$. After the time interval 5×10^6 $\tau = 1000T$, all thermally cycled and

aged samples were strained along the $\hat{x}$ direction up to $\varepsilon_{xx} = 0.5$. The stress–strain response is summarized in Fig. 9 for four cooling rates and selected values of the thermal cycling amplitude. It can be seen that glasses that are more slowly annealed and then aged at $T_{LJ} = 0.01\varepsilon/k_B$ exhibit a more pronounced yield stress peak (black curves in Fig. 9). With increasing maximum temperature up to $T_{LJ} = 0.35\varepsilon/k_B$, the yielding peak increases in all four cases shown in Fig. 9. Note also that the maximum stress is approximately the same for all cooling rates when $T_{LJ} = 0.35\varepsilon/k_B$. Similar conclusions were obtained in the previous study, despite that simulations were performed for fewer values of the thermal cycling amplitude and the steady state was not reached [30].

We finally plot the values of the yielding peak, elastic modulus, and the minima of the potential energy after 1000 thermal cycles in Fig. 10 as a function of the maximum temperature. It can be observed that with increasing thermal cycling amplitude, both σ_Y and E increase, except for the case $T_{LJ} = 0.4\varepsilon/k_B$. Thus, the maximum of the yield stress and elastic modulus is acquired in glasses thermally cycled with the amplitude $T_{LJ} = 0.35\varepsilon/k_B$. These trends are inversely correlated with the variation of the potential energy minima shown in the inset (a) in Fig. 10. The origin of a slight upward curvature in U $(1000T)$ for the well-annealed glass at small T_{LJ} is at present not clear. Given that the potential energy in all samples in Fig. 6 saturates to a constant level after several hundred cycles, we conclude that the results for mechanical properties presented in Fig. 10 should be independent of the cycle number.

Conclusions

In summary, the effect of periodic thermal treatment on structural relaxation and mechanical properties of binary glasses was investigated using MD simulations. We considered the Kob–Andersen binary mixture annealed across the glass transition with different cooling rates and subjected to repeated heating and cooling cycles at constant pressure. It was found that during a few hundred transient cycles, the potential energy minima gradually decrease toward a steady state with the lowest energy level, which depends on the thermal cycling amplitude. Moreover, with increasing thermal amplitude up to a certain value, the number of transient cycles decreases and the level of the potential energy is reduced. The structural relaxation proceeds by collective, nonaffine displacements of atoms that are organized into clusters. In contrast, the particle dynamics in steady state becomes nearly reversible and the system returns to the same energy state after each thermal cycle. The results of tensile tests after one thousand cycles revealed that the maximum values of the elastic modulus and yielding peak occur at the same thermal cycling amplitude regardless of the annealing history.
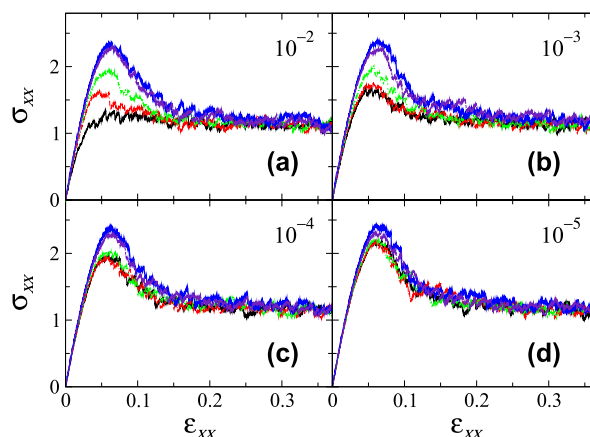

Figure 9: The tensile stress σ_{xx} (in units of $\varepsilon\sigma^{-3}$) versus strain for glasses prepared with cooling rates (a) 10^{-2} $\varepsilon/k_B\tau$, (b) 10^{-3} $\varepsilon/k_B\tau$, (c) 10^{-4} $\varepsilon/k_B\tau$, and (d) 10^{-5} $\varepsilon/k_B\tau$. The data for glasses aged at $T_{LJ} = 0.01\varepsilon/k_B$ are indicated by solid black curves. The stress–strain response for glasses thermally cycled with the maximum temperature $0.1\varepsilon/k_B$ (dashed-dotted red), $0.2\varepsilon/k_B$ (dotted green), $0.35\varepsilon/k_B$ (dark solid blue), and $0.4\varepsilon/k_B$ (dashed indigo). The samples were strained with the rate $\dot{\varepsilon}_{xx} = 10^{-5}\tau^{-1}$ at $T_{LJ} = 0.01\varepsilon/k_B$ and $P = 0$.
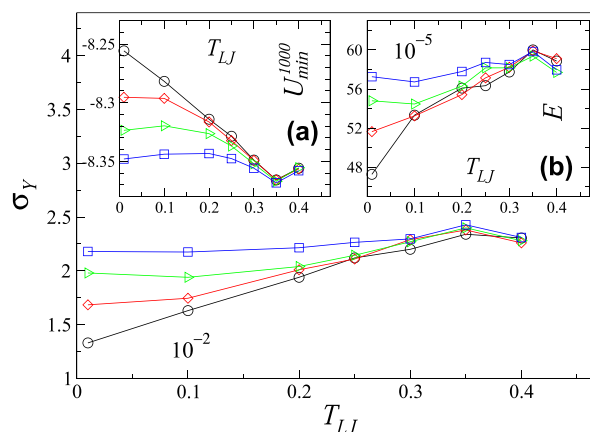

Figure 10: The yielding peak σ_Y (in units of $\varepsilon\sigma^{-3}$) as a function of the thermal amplitude for cooling rates 10^{-2} $\varepsilon/k_B\tau$ ($\bigcirc$), 10^{-3} $\varepsilon/k_B\tau$ ($\diamond$), 10^{-4} $\varepsilon/k_B\tau$ ($\triangleright$), and 10^{-5} $\varepsilon/k_B\tau$ ($\square$). The inset (a) shows the potential energy minima after 1000 thermal cycles. The inset (b) displays the elastic modulus E (in units of $\varepsilon\sigma^{-3}$) versus the thermal amplitude for the same samples and cooling rates.

In the future, it might be instructive to investigate whether the details of thermal treatment, such as the reference temperature, oscillation period, system size, and choice of atomistic model, will affect the main conclusions regarding the potential energy states and mechanical properties of amorphous materials. One of the findings of this study is the appearance of well-defined steady states with particular energy levels and nearly reversible dynamics. This, in turn, opens the question of memory formation in such systems similar to memory effects reported in periodically driven glasses [39]. For example, thermally cycled glasses with a particular thermal amplitude

might continue to expand and contract reversibly if the thermal amplitude is reduced or instead undergo structural relaxation if the thermal amplitude is increased.

Acknowledgments

Supplementary material

To view supplementary material for this article, please visit https://doi.org/10.1557/jmr.2019.145.

References

1. **C. Liu and R. Maass**: Elastic fluctuations and structural heterogeneities in metallic glasses. *Adv. Funct. Mater.* **28**, 1800388 (2018).

2. **A.S. Argon**: Plastic deformation in metallic glasses. *Acta Metall.* **27**, 47 (1979).

3. **F. Spaepen**: A microscopic mechanism for steady state inhomogeneous flow in metallic glasses. *Acta Metall.* **25**, 407 (1977).

4. **T. Egami, T. Iwashita, and W. Dmowski**: Mechanical properties of metallic glasses. *Metals* **3**, 77 (2013).

5. **E.S. Park and D.H. Kim**: Phase separation and enhancement of plasticity in Cu–Zr–Al–Y bulk metallic glasses. *Acta Mater.* **54**, 2597 (2006).

6. **H-K. Kim, J-P. Ahn, B-J. Lee, K-W. Park, and J-C. Lee**: Role of atomic-scale chemical heterogeneities in improving the plasticity of Cu–Zr–Ag bulk amorphous alloys. *Acta Mater.* **157**, 209 (2018).

7. **B. Sarac and J. Schroers**: Designing tensile ductility in metallic glasses. *Nat. Commun.* **4**, 2158 (2013).

8. **S.V. Ketov, Y.H. Sun, S. Nachum, Z. Lu, A. Checchi, A. R. Beraldin, H.Y. Bai, W.H. Wang, D.V. Louzguine-Luzgin, M. A. Carpenter, and A.L. Greer**: Rejuvenation of metallic glasses by non-affine thermal strain. *Nature* **524**, 200 (2015).

9. **A.L. Greer and Y.H. Sun**: Stored energy in metallic glasses due to strains within the elastic limit. *Philos. Mag.* **96**, 1643 (2016).

10. **W. Song, X. Meng, Y. Wu, D. Cao, H. Wang, X. Liu, X. Wang, and Z. Lu**: Improving plasticity of the $Zr_{46}Cu_{46}Al_8$ bulk metallic glass via thermal rejuvenation. *Sci. Bull.* **63**, 840 (2018).

11. **D. Grell, F. Dabrock, and E. Kerscher**: Cyclic cryogenic pretreatments influencing the mechanical properties of a bulk glassy Zr-based alloy. *Fatigue Fract. Eng. Mater. Struct.* **41**, 1330 (2018).

12. **W. Guo, R. Yamada, and J. Saida**: Rejuvenation and plasticization of metallic glass by deep cryogenic cycling treatment. *Intermetallics* **93**, 141 (2018).

13. **S.V. Ketov, A.S. Trifonov, Y.P. Ivanov, A.Y. Churyumov, A. V. Lubenchenko, A.A. Batrakov, J. Jiang, D.V. Louzguine-Luzgin, J. Eckert, J. Orava, and A.L. Greer**: On cryothermal cycling as a method for inducing structural changes in metallic glasses. *NPG Asia Mater.* **10**, 137 (2018).

14. **B. Shang, P. Guan, and J-L. Barrat**: Role of thermal expansion heterogeneity in the cryogenic rejuvenation of metallic glasses. *J. Phys.: Mater.* **1**, 015001 (2018).

15. **M. Utz, P.G. Debenedetti, and F.H. Stillinger**: Atomistic simulation of aging and rejuvenation in glasses. *Phys. Rev. Lett.* **84**, 1471 (2000).

16. **D.J. Lacks and M.J. Osborne**: Energy landscape picture of overaging and rejuvenation in a sheared glass. *Phys. Rev. Lett.* **93**, 255501 (2004).

17. **N.V. Priezjev**: Heterogeneous relaxation dynamics in amorphous materials under cyclic loading. *Phys. Rev. E* **87**, 052302 (2013).

18. **D. Fiocco, G. Foffi, and S. Sastry**: Oscillatory athermal quasistatic deformation of a model glass. *Phys. Rev. E* **88**, 020301(R) (2013).

19. **I. Regev, T. Lookman, and C. Reichhardt**: Onset of irreversibility and chaos in amorphous solids under periodic shear. *Phys. Rev. E* **88**, 062401 (2013).

20. **N.V. Priezjev**: Dynamical heterogeneity in periodically deformed polymer glasses. *Phys. Rev. E* **89**, 012601 (2014).

21. **I. Regev, J. Weber, C. Reichhardt, K.A. Dahmen, and T. Lookman**: Reversibility and criticality in amorphous solids. *Nat. Commun.* **6**, 8805 (2015).

22. **N.V. Priezjev**: Reversible plastic events during oscillatory deformation of amorphous solids. *Phys. Rev. E* **93**, 013001 (2016).

23. **N.V. Priezjev**: Nonaffine rearrangements of atoms in deformed and quiescent binary glasses. *Phys. Rev. E* **94**, 023004 (2016).

24. **P. Leishangthem, A.D.S. Parmar, and S. Sastry**: The yielding transition in amorphous solids under oscillatory shear deformation. *Nat. Commun.* **8**, 14653 (2017).

25. **N.V. Priezjev**: Collective nonaffine displacements in amorphous materials during large-amplitude oscillatory shear. *Phys. Rev. E* **95**, 023002 (2017).

26. **M. Fan, M. Wang, K. Zhang, Y. Liu, J. Schroers, M.D. Shattuck, and C.S. O'Hern**: The effects of cooling rate on particle rearrangement statistics: Rapidly cooled glasses are more ductile and less reversible. *Phys. Rev. E* **95**, 022611 (2017).

27. **N.V. Priezjev**: Molecular dynamics simulations of the mechanical annealing process in metallic glasses: Effects of strain amplitude and temperature. *J. Non-Cryst. Solids* **479**, 42 (2018).

28. **N.V. Priezjev**: The yielding transition in periodically sheared binary glasses at finite temperature. *Comput. Mater. Sci.* **150**, 162 (2018).

29. **M. Blank-Burian and A. Heuer**: Shearing small glass-forming systems: A potential energy landscape perspective. *Phys. Rev. E* **98**, 033002 (2018).

30. **N.V. Priezjev**: The effect of cryogenic thermal cycling on aging, rejuvenation, and mechanical properties of metallic glasses. *J. Non-Cryst. Solids* **503–504**, 131 (2019).

31. **W. Kob and H.C. Andersen**: Testing mode-coupling theory for a supercooled binary Lennard-Jones mixture: The van Hove correlation function. *Phys. Rev. E* **51**, 4626 (1995).

32. **T.A. Weber and F.H. Stillinger**: Local order and structural transitions in amorphous metal-metalloid alloys. *Phys. Rev. B* **31**, 1954 (1985).

33. **M.P. Allen and D.J. Tildesley**: *Computer Simulation of Liquids* (Clarendon, Oxford, 1987).

34. **S.J. Plimpton**: Fast parallel algorithms for short-range molecular dynamics. *J. Comput. Phys.* **117**, 1 (1995).

35. **M.D. Ediger and P. Harrowell**: Perspective: Supercooled liquids and glasses. *J. Chem. Phys.* **137**, 080901 (2012).

36. **W. Kob and J-L. Barrat**: Fluctuations, response and aging dynamics in a simple glass-forming liquid out of equilibrium. *Eur. Phys. J. B* **13**, 319 (2000).

37. **M.L. Falk and J.S. Langer**: Dynamics of viscoplastic deformation in amorphous solids. *Phys. Rev. E* **57**, 7192 (1998).

38. **N.V. Priezjev**: Slow relaxation dynamics in binary glasses during stress-controlled, tension-compression cyclic loading. *Comput. Mater. Sci.* **153**, 235 (2018).

39. **N.C. Keim, J. Paulsen, Z. Zeravcic, S. Sastry, and S.R. Nagel**: Memory formation in matter. arXiv:1810.08587 (2018).